Replication of viruses in a growing plaque: a reaction-diffusion model

John Yin and J. S. McCaskill
Department of Biochemical Kinetics, Max-Planck-Institute for Biophysical Chemistry, W-3400 Göttingen, Germany

ABSTRACT An understanding of the viral replication process commonly referred to as "plaque growth" is developed in the context of a reaction-diffusion model. The interactions among three components: the virus, the healthy host, and the infected host are represented using rates of viral adsorption and desorption to the cell surface, replication and release by host lysis, and diffusion. The solution to the full model reveals a maximum in the dependence of the velocity of viral propagation on its equilibrium adsorption constant, suggesting that conditions can be chosen where viruses which adsorb poorly to their hosts will replicate faster in plaques than those which adsorb well.

Analytic expressions for the propagation velocity as a function of the kinetic and diffusion parameters are presented for the limiting cases of equilibrated adsorption, slow adsorption, fast adsorption, and large virus yields. Hindered diffusion at high host concentrations must be included for quantitative agreement with experimental data.

INTRODUCTION

We are developing experimental systems to better understand the role environmental factors play in the growth and evolution of viruses. The major challenge is to continuously provide replicating viruses with receptive hosts. Traditionally, this problem has been overcome using serial transfer techniques (1–3): an initial stock of viruses is mixed with host cells and permitted to replicate; then a small volume is removed and transferred to a new vessel containing fresh host, the infection is repeated and the process is continued indefinitely. A cascaded flow-reactor system based on this principle has also been developed (4, 5): a continuous culture of the host organism is pumped through a stirred flow-through vessel where replicating viruses are diluted. Both methods are limited in the kind of information they can provide. The technical difficulty of measuring viral properties instantaneously combined with variations in the concentration and metabolic state of the host cells prevent the direct observation of novel phenotypes as they arise. During propagation in plaques, however, the continuous replication, mutation and selection of viruses may be observed and perhaps even controlled.

A plaque is a region of lysed host cells, visible to the unaided eye, and formed by the growth of viruses in a thin layer of agar containing their evenly distributed receptive host cells. The growth process is initiated when a free virus particle diffuses to a host cell, adsorbs to its surface, replicates within, and finally lyses it, releasing a new generation of infective particles, which then diffuse to neighboring hosts and repeat the process. The velocity of viral propagation is easily and precisely determined by monitoring plaque sizes over several hours or days. Although assays based on the plaque-forming ability of viruses have served more than sixty years to characterize and quantify viruses (6–8), and plaques containing mixed phenotypes and genotypes have been observed (9, 10), plaque growth has not yet been widely recognized as a means for studying evolutionary processes.

Our interest in understanding plaque growth was sparked by the recent observation that during growth, wild type viruses subjected to a very specific environmental condition can give rise to mutants which outgrow their precursors. When wild type bacteriophage T7 was grown on a bacterial host which provided the T7 RNA polymerase, mutants lacking this gene but requiring the host-provided enzyme for growth arose and outgrew the original wild type (manuscript in preparation). The emergence of these mutants correlated with bulged regions along the plaque boundary, regions where the viral propagation were presumably enhanced. How the deletion of a gene granted the variants an advantage over the wild type is not yet known.

Our goal here is to derive an explicit expression for the macroscopic observable, the rate of plaque growth, in terms of the microscopic kinetic and diffusion parameters and the host concentration. By studying the effects of agar concentration and host colony spacing on plaque growth, early investigators suggested that diffusive and kinetic mechanisms were both important for determining the rate of plaque growth (6, 11). Later, Koch developed a model which suggested, using heuristic

0006-3495/92/06/1540/10 $2.00

arguments, that the rate of plaque growth should be approximately constant and dependent on the viral diffusivity and the lag time for viral replication in the infected host; he also provided modifications to his model to account for reversible or irreversible viral adsorption mechanisms (12). Our approach follows one developed recently for an in vitro system: the coupled replication and diffusion of RNA molecules propagating along a capillary (13). We derive the differential equations which describe the radial position and time dependence of three components: the viruses, the host and the infected host during plaque growth. For a constant rate of growth or constant velocity of radial propagation, we obtain a traveling-wave solution where the velocity is governed by the microscopic reaction rates and viral diffusivity.

Experimental data obtained for the propagation velocity dependence on the host concentration displayed an unexpected effect: at high host concentrations the plaques grew more slowly. While the model exhibits such a qualitative behavior, no fit to the rapid fall off at high concentrations could be made. By considering how the inert volume occupied by the hosts under these conditions could reduce the effective viral diffusivity, the model could account for this behavior.

METHODS

Theoretical

Front velocity

We model the plaque growth process by considering the interactions among three species, the free virus particle (V), the host bacteria (B) and the infected host bacteria (I), which results from the adsorption of the virus particle to the host. The reactions involved may be summarized as follows:

$$V + B \underset{k_{-1}}{\overset{k_1}{\rightleftharpoons}} I \xrightarrow{k_2} \mathrm{Y} \cdot V, \tag{1}$$

where k_1 and k_{-1} are rate constants of adsorption and desorption for the virus particle to its host, respectively, k_2 is the rate constant for death (or lysis) of the infected host and Y is the yield of new viruses produced per lysed host. We neglect the adsorption of viruses to infected host, assume the virus particles diffuse with coefficient D in the agar medium, and that the hosts are not able to diffuse. Because the plaques are radially symmetric, we work in polar coordinates and write down the reaction-diffusion equations for the three concentrations (given in brackets [ ]) as functions of position (r) and time (t):

$$\frac{\partial[V]}{\partial t} = D\frac{\partial^2[V]}{\partial r^2} + \frac{D}{r}\left(\frac{\partial[V]}{\partial r}\right) - k_1[V][B] + k_{-1}[I] + \mathrm{Y}k_2[I] \tag{2a}$$

$$\frac{\partial[B]}{\partial t} = -k_1[V][B] + k_{-1}[I] \tag{2b}$$

$$\frac{\partial[I]}{\partial t} = k_1[V][B] - k_{-1}[I] - k_2[I], \tag{2c}$$

with boundary conditions $r(\partial[V]/\partial r) = 0$ at $r = 0$; and $[V] = 0$, $[B] = B_0$ and $[I] = 0$ as $r \to \infty$. For initial conditions corresponding to localized viral infection, we take for simplicity a small disk radius, R_0, inside which all bacteria are infected. The term, $(1/r)\partial[V]/\partial r$ is significant only for situations where highly curved or very diffuse plaque boundaries occur; we neglect this term for the moment and quantify these conditions in Appendix 1. The equations are cast in dimensionless variables by defining $\overline{V} \equiv [V]/B_0$, $\overline{B} \equiv [B]/B_0$, $\overline{I} \equiv [I]/B_0$, $\bar{t} \equiv k_2 t$ and $\bar{r} \equiv (k_2/D)^{1/2} r$. We look for a traveling-wave solution satisfying a set of ordinary differential equations in the coordinate, $\bar{z} \equiv \bar{r} - \bar{c}\bar{t}$, which moves at the dimensionless velocity of the propagating front, $\bar{c}$, where $\bar{c} = c/(k_2 D)^{1/2}$. In addition, we consider the concentrations of each of the components at the leading edge of the front. As the components approach their limiting concentrations, the linearized form of Eq. 2 becomes valid, and solutions following an exponential dependence hold: $\overline{V} = a_1 \exp(-\xi\bar{z})$, $\overline{B} = (1 - a_2 \exp(-\xi\bar{z}))$ and $\overline{I} = a_3 \exp(-\xi\bar{z})$ where $(1/\xi)$ is the dimensionless decay length (or characteristic width) of the front and a_1, a_2 and a_3 are positive constants. Substitution into Eq. 2 and rewriting in the matrix notation yields

$$\begin{pmatrix} \xi^2 - \bar{c}\xi - \kappa_1 & 0 & \kappa_{-1} + \mathrm{Y} \\ -\kappa_1 & \bar{c}\xi & \kappa_{-1} \\ \kappa_1 & 0 & -\bar{c}\xi - \kappa_{-1} - 1 \end{pmatrix} \begin{pmatrix} a_1 \\ a_2 \\ a_3 \end{pmatrix} = 0, \tag{3}$$

where $\kappa_1 \equiv k_1 B_0/k_2$ and $\kappa_{-1} \equiv k_{-1}/k_2$. For a nontrivial solution the determinant of the matrix is set to zero, expanded and simplified:

$$g(\xi) \equiv \xi^3 + C_1\xi^2 + C_2\xi + C_3 = 0, \tag{4}$$

where $C_1 = [(\kappa_{-1} + 1)/\bar{c} - \bar{c}]$, $C_2 = -(\kappa_1 + \kappa_{-1} + 1)$ and $C_3 = \kappa_1(\mathrm{Y} - 1)/\bar{c}$. Because the concentrations must be positive and real, we require that the dimensionless velocity, $\bar{c}$, satisfies conditions such that a solution to Eqs. 3 and 4 with ξ, a_1, a_2, a_3 positive and real exists. From the reasoning given in Appendix 1, the minimum velocity $\bar{c}$ is given by the condition that the discriminant of $g(\xi)$ equals zero. Given the radial-step initial conditions of Eq. 2, we expect the solution to converge to a wave traveling at the minimal velocity, following a generalization of arguments given for one dimensional one- and two-component cases (14, 15). After substitution, expansion and simplification, the critical condition takes the form,

$$b_1X^3 + b_2X^2 + b_3X + b_4 = 0, \tag{5a}$$

where $X \equiv \bar{c}^2$. The coefficients depend on the kinetic parameters as follows:

$$b_1 = -[(K + 1)\kappa_{-1}]^2 + 2[K(1 - 2\mathrm{Y}]) - 1](\kappa_{-1}) - 1 \tag{5b}$$

$$b_2 = -2[(K + 1)^2(2K + 1)(\kappa_{-1})^3 - [K^2(4 - 9\mathrm{Y}) - K(3\mathrm{Y} + 5) - 3](\kappa_{-1})^2 + 2[K(3\mathrm{Y} + 1) + 3](\kappa_{-1}) + 1] \tag{5c}$$

$$b_3 = -(K + 1)^2(\kappa_{-1})^4 + 2[K^2(9\mathrm{Y} - 10) + 3K(\mathrm{Y} - 2) - 2](\kappa_{-1})^3 + [K^2(27\mathrm{Y}^2 - 36\mathrm{Y} + 8) + 6K(2\mathrm{Y} - 3) - 6](\kappa_{-1})^2 + 2[K(3\mathrm{Y} - 4) - 2](\kappa_{-1}) - 1 \tag{5d}$$

$$b_4 = 4K(\mathrm{Y} - 1)(\kappa_{-1})(\kappa_{-1} + 1)^3, \tag{5e}$$

where $K \equiv \kappa_1/\kappa_{-1}$ is a dimensionless equilibrium constant for adsorption. Because b_4 is positive here and both b_1 and b_2 are negative, there exists only one positive root for this expression, which gives the limiting velocity squared. Analytic expressions for Eq. 5 are cumbersome. We therefore obtain explicit expressions for the velocity under the limiting conditions given below.

Equilibrated adsorption

When the viral adsorption and desorption processes are fast relative to the death rate of the infected host (κ_{-1} large for fixed K), b_3X and b_4 give a dominant balance, and the velocity, c_{EQ}, is readily obtained:

$$c_{EQ} = 2\left[\frac{Dk_2(Y-1)f\cdot K_{max}}{(f\cdot K_{max}+1)^2}\right]^{1/2}, \qquad (6a)$$

where $K_{max} \equiv k_1B_{max}/k_{-1}$, $f \equiv B_0/B_{max}$, and B_{max} is the maximum value attainable by B_0. Thus, $f\cdot K_{max}$, attains its maximum value when f, the host fraction, is unity. By introducing B_{max}, we see how the virus's inherent binding affinity and the host concentration, reflected in K_{max} and f, respectively, separately influence the velocity. This representation will become particularly useful when we consider the effects of hindered diffusion and fit experimental data.

Large yield

For the situation where the yield (Y) of new virus particles per infected host is large, a dominant balance is obtained between the b_1X^3 and b_3X terms, and the velocity c_Y, is given by

$$c_Y = \left[\frac{3D}{2}(3k_1fB_{max}k_2Y)^{1/2}\right]^{1/2}, \qquad (6b)$$

where again, B_{max} (and f) have been introduced to show explicitly the dependence of the velocity on the host concentration. Additional limiting cases are recorded in Appendix 2.

Hindered diffusion

The diffusion of the virus particles has implicitly been assumed to occur in a homogeneous medium. In reality, the host bacteria may, in addition to catalyzing the viral replication, act as a diffusional barrier, depending on the volume fraction of the medium it occupies. We may account for this effect by determining the diffusivity of a solute through a suspension of diffusionally impermeable spheres (16, 17):

$$\frac{D_{eff}}{D} = \frac{2(1-f)}{2+f}, \qquad (7)$$

where D_{eff} is the effective diffusivity, D is the solute diffusivity in the continuous phase, and f is the volume fraction occupied by the impermeable spheres, in our case, the host bacterial microcolonies. Assuming the volume fraction of the host is proportional to its concentration, f will equal B_0/B_{max}, as above, where B_{max} equals the bacterial concentration required to completely occupy the diffusional medium.

Experimental

Established procedures were employed in the preparation, preservation and concentration determinations of the bacteriophage and the bacteria (7, 18, 19). The wild-type strain of phage T7 as well as the host strain BL21 (F^- *hsdS gal*) of Escherichia coli were obtained as generous gifts from F. W. Studier.

Single-layer plates containing agar, nutrient broth for bacterial growth and host bacteria were prepared as described elsewhere (20). The stock nutrient broth (Merck, Nutrient broth DAB 7) is a rich medium containing on a weight percent basis 25% infusion from meat, 50% peptone from meat, 10% di-sodium hydrogen phosphate and 15% sodium chloride. Concentrations ranged from 4 to 50 grams of nutrient broth per liter plating mix (agar, broth, host bacteria and virus particles). T7 plaques were initiated by stabbing the surface of the gelled agar mix with a needle which had been dipped in a diluted stock solution of T7 (10^7 plaque forming units/ml). Similar results were obtained when plaques were initiated by single virions. Plaque diameters were measured beginning after 12 h incubation at 37°C. Four measurements were made for each plaque at four hour intervals. The front velocity was calculated from the slope of the linear regression fit for the plaque diameter versus time. An average velocity was determined for at least five and in most cases six growing plaques at each nutrient broth and initial host concentration.

RESULTS

Velocity dependence on viral adsorption

In theory, the velocity of viral propagation can depend on the viral diffusivity (D), the kinetic parameters for absorption (k_1), desorption (k_{-1}), and replication/lysis (k_2), the average yield of active virus particles per infected host (Y), and the host concentration (B_0 or f). By considering the plaque growth process in the context of a reaction-diffusion model we may better understand how each of these parameters contributes to the observable propagation.

The full dependence of the velocity on the system's parameters, given implicitly in Eq. 5, although cumbersome, exhibits two important features. First, because diffusional effects only enter the equations through X (equal to c^2/Dk_2), the velocity always scales with the square root of the viral diffusivity, $D^{1/2}$. Second, the velocity dependence on the viral adsorption has a maximum, as shown in Fig. 1 *a* for fixed Y over a range of κ_{-1}. This result can be understood by considering the large κ_{-1} limit.

At fixed K, varying κ_{-1} alters the speed with which the viral adsorption equilibrium is attained. In the limit of large κ_{-1} an equilibrium between absorbed and unadsorbed viruses is reached and the velocity becomes independent of κ_{-1}; Fig. 1 *a* shows a close approximation to this limit for the curve log (κ_{-1}) equal to four. We now restrict our attention to the behavior of the velocity for large κ_{-1} over a broad range of K, the dimensionless equilibrium adsorption constant. If K is small (log (K) less than zero in Fig. 1 *a*), then adsorption is slow. Increasing K has the effect of increasing, κ_1 or B_0; the resulting faster adsorption produces a higher velocity, as one might intuitively expect. However, when the viral adsorption rate is already large, increasing it further

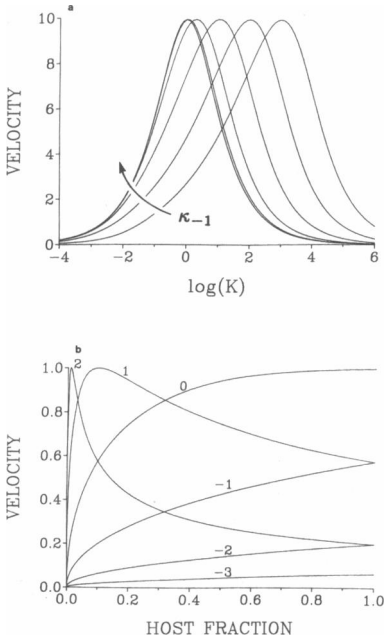

FIGURE 1 (*a*) Velocity dependence on parameters K and κ_{-1}. The dependence of the dimensionless velocity $\bar{c}$ on κ_{-1} and K is shown for the full solution to Eq. 5. κ_{-1}, which is proportional to the desorption rate, is shown in log units from -1 to 4. K is a measure of viral adsorption, proportional to both the inherent affinity of the virus for its host as well as the host concentration. At fixed K, increasing κ_{-1} increases the rate of adsorption. The host yield Y is fixed at 100. (*b*) Velocity dependence on host fraction. Assuming equilibrated adsorption, curves are shown for values of the inherent adsorption constant spanning five orders of magnitude ($\log K_{max}$ from -3 to 2). The velocity has been normalized with respect to the maximum velocity of the curve for $\log K_{max} = 2$, and the host fraction has been defined as the host concentration, B_0 normalized with respect to an unspecified large host concentration, B_{max}.

reduces the velocity by depleting the pool of freely diffusing viruses needed for propagation.

In practice, the experimentally observed velocity of propagation may be limited by a specific reaction step, in which case, Eq. 5 may be reduced to an explicit expression for the velocity. Such expressions provide not only a pragmatic bridge to experimental studies, but also help the experimentalist focus on potentially rate determining processes. Above, the equilibrated adsorption or large κ_{-1} limit provided a means for understanding the maximum in the dependence of the velocity on K; an analytical expression in this limit is derived in Eq. 6*a*; here, K has been replaced by $f \cdot K_{max}$ in order to separate the effects of host concentration and inherent binding affinity. The behavior is depicted in Fig. 1 *b* over the entire range of host concentrations: for f from zero to one; the dependence on K_{max} is plotted for values spanning five orders of magnitude, from 10^{-3} to 10^{2}.

Each of the curves in Fig. 1 *b* is a portion of the curve obtained for the large κ_{-1} limit shown in Fig. 1 *a*. The size of the portion depends on the value of K_{max}. For example, the curve for K_{max} equal to 0.1 in Fig. 1 *b* corresponds to the portion of the curve ranging from K equal to zero (not shown, but approximated by log (K) equal to -4) to 0.1. The monotonic dependence of the velocity on f in Fig. 1 *b* corresponds to the dependence on K in Fig. 1 *a*. This dependence obtains for values of K_{max} up to 1. At larger values the curve passes through a maximum corresponding to the maximum in Fig. 1 *a*. In addition, taking larger K_{max} values shifts the position of the maximum toward smaller host fractions in Fig. 1 *b* or smaller K values in Fig. 1 *a*.

Analytic expressions for the velocity in the limits of small and large K_{max} are readily derived and presented in Appendix 2. For small K_{max} the behavior approaches the slow adsorption limit, and the velocity increases monotonically with the host fraction, f, as expected. For large K_{max} the behavior approaches the fast adsorption limit, and the velocity decreases monotonically with the host fraction.

Effect of hindered diffusion

The apparently pedestrian role played by the viral diffusivity, a $D^{1/2}$ contribution to the front velocity in all cases, becomes potentially important when we account for the finite volume the hosts occupy in the transport medium. When occupying large volumes they decrease the space available for viral diffusion; paths for diffusion become more tortuous, effectively reducing the diffusivity. This effect may be accounted for by assuming that the maximum host concentration attainable, defined by B_{max}, corresponds to a host volume which completely fills the transport medium and thereby prevents diffusion. The viral diffusivity, D, in Eq. 6 is then replaced by an effective diffusivity, dependent on the host fraction, f, as provided in Eq. 7.

From the form of Eq. 7 it is evident that the major effect of hindered diffusion, when defined with respect to the host volume fraction, is to force the velocity through zero at a host fraction of unity. For small host fractions the velocity behaves as in Fig. 1 *b* because the host-occupied volume is negligible. However, as the fraction increases, hindered diffusion effects come into play and the velocity, even for small K_{max}, goes through a maximum, as seen in Fig. 2.

Experimental results

A comparison of the theoretical model with experimental data collected for the growth of bacteriophage T7 at different host fractions is presented in Fig. 3 *a*. We have assumed that the host fraction, f or B_0/B_{max}, is propor-

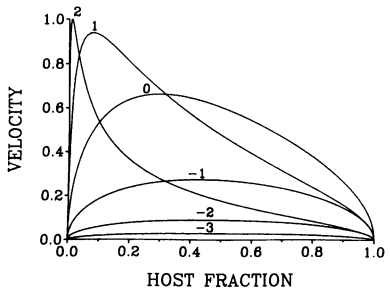

FIGURE 2 Influence of hindered diffusion on the velocity. Assuming equilibrated adsorption, curves are shown for values of the inherent adsorption constant spanning five orders of magnitude (log K_{max} from −3 to 2). The velocity has been normalized with respect to the maximum velocity of the curve for log K_{max} = 2, and the host fraction has been defined as the volume fraction occupied by the host.

tional to the concentration of nutrient broth used in experiments. This implies that a critical nutrient concentration (~50 g/l in this work) corresponding to a host fraction of unity exists; as the host fraction approaches unity the velocity approaches zero due to the reduced effective diffusivity of the virus particles. Although the host bacteria was plated at initial concentrations of 10^7/ml and 10^8/ml, these initial differences had no apparent effect on the front velocities over a range of host fractions, suggesting that the host fraction (or nutrient broth concentration) and not the initial concentration of host cells used for plating determine f (or B_0), the host concentration for the model.

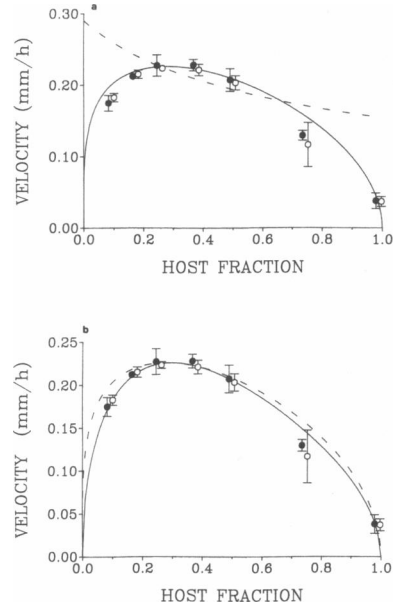

FIGURE 3 (*a*) Two-parameter models fit to experimental data. The dotted curve represents the behavior of Koch's model accounting for the effects of reversible adsorption. The filled curve represents the behavior of the large-yield/hindered diffusion approximation of this work. The open and closed data symbols refer to initial cell concentrations of 10^7/ml and 10^8/ml, respectively. (*b*) Two- and three-parameter models fit to experimental data. The dotted curve is the best two-parameter fit for the large-yield/hindered-diffusion approximation of this work. The filled curve is the best three-parameter fit for the equilibrated-adsorption/hindered-diffusion approximation of this work (for log K_{max} = 0.11). The open and closed data symbols refer to initial cell concentrations of 10^7/ml and 10^8/ml, respectively.

Two models, both allowing two adjustable parameters, are shown. The first, depicted by a smooth curve which reaches a maximum near a host fraction of 0.3, represents the large-yield approximation with hindered diffusion. The major features of the experimental results appear to be captured: a steep rise of the velocity with the host fraction followed by a gradual descent.

The second theoretical model of Fig. 3 *a*, depicted by a monotonically decreasing dotted curve, represents the behavior of Koch's heuristic model modified to account for the effects of reversible adsorption (12). Koch developed his model under the restricted conditions where the maximum velocities in Fig. 3*a* were found to occur; conditions where host fractions are sufficiently large that freshly replicated viruses can diffuse to neighboring hosts during a lag time (inversely proportional to k_2), yet not so concentrated that they interfere with the viral diffusion. Hence, his model is unable to capture the strong dependence of the velocity over the entire range of the host fraction.

Finally, a comparison of the equlibrated-adsorption and large-yield models is shown in Fig. 3 *b*. As expected, the equlibrated-adsorption model, using its additional degree of freedom, (K_{max}), can more closely match the experimental results. The overestimate of the velocity by the large-yield model at low host fractions is not unexpected. At low host fractions, the virus yields will also be small, and the assumption that a large yield dominates is not readily justified. More likely, and also supported by the better fit of the equilibrated-adsorption model, the adsorption rate plays an important role at low host fractions. The small differences between the large-yield and equilibrated-adsorption models at high host fractions are also revealing. From the curves in Fig. 3 *b* it is clear that the effect of hindered diffusion dominates any assumptions regarding the replication kinetics.

Predicting the front velocity

A lack of information about the virus/host interactions in agar currently prevents a reliable a priori estimation of the front velocity. However, the overestimate obtained by using parameters from single-burst shaker cultures (7, 12) may serve as a useful point of departure. For a lag time of 13 min (21) one may calculate k_2 equal

to 6/h. Yields (Y) under optimal conditions are ~200 active phages per infected host (22). Assuming the equilibrium adsorption constant for phage T1 holds for T7, k_1/k_{-1} is 3×10^{-8} cm^3 (23). For the initial host concentration, B_0 equal to 1.5×10^7/ml and a diffusivity for T7-shaped particles (using the data for phage P22, which approximates T7 in shape and size [24]) in 10 g/l agar of 4×10^{-8} cm^2/s (25), we obtain from Eq. 6*a*, a front velocity of 4 mm/h, which is 20-fold higher than the maximum experimentally determined velocity shown in Fig. 3 *a*.

A partial explanation for disprepancies between the predicted and experimentally measured velocities may be provided by determining the phage yields within a plaque. The yield from an agar-immobilized microcolony containing 10^1 to 10^5 individual host cells is apparently less than the yield from an individual infected cell under optimal growth conditions. From the maximum free phage concentration in a growing plaque (10^{10}/ml) and a microcolony concentration (2.4×10^8/ml) (20) one obtains an effective yield of only 40 active phages per microcolony. Several factors may account for the poor yield: inherently lower yields per cell when immobilized in agar, premature lysis or inhibition of cells due to the death of adjacent cells, high multiplicities of adsorption required for host infection, or readsorption of newly released particles on cell fragments.

Predicting the decay length

The theoretical model suggests that a length scale associated with the leading edge of the propagating front, like the front velocity itself, will depend on the parameters of viral diffusion and replication. This decay length, $\lambda \equiv (D/k_2)^{1/2}(1/\xi)$, is strictly defined only at positions in the front where concentrations approach their limiting values, that is, where the linearized forms of Eq. 2 hold. It is conceivable, however, that a camera capable of quantifying light intensities with good spacial resolution could provide experimental data which could be correlated to decay lengths.

Theoretical expressions for the decay length are presented under various limiting conditions as shown in Eq. A10–14 of Appendix 3. In all cases, except for fast adsorption, the decay length is proportional to (D/c), the viral diffusivity divided by the front velocity. For a diffusivity of 4×10^{-8} cm^2/s and a typical velocity of 0.22 mm/h, the slow adsorption and large-yield assumptions both give a decay length of ~0.1 mm.

In the equilibrated-adsorption limit the decay length also depends on K_{max}, the inherent adsorption constant, as given in Eq. A11. Assuming the diffusivity and the host fraction are known and remain constant, one could estimate K_{max} by measuring the velocity and the decay length in the growing plaque. Similarly, under conditions where the fast adsorption limit holds, the velocity and decay length constrain k_2Y as given in Eq A13.

DISCUSSION

The good agreement between the experimental data and two theoretical results shown in Fig. 3 *b* demonstrates that the model accounts for the peculiar dependence of the plaque growth rate on the host fraction. At low fractions the velocity rises monotonically because infected hosts are required to maintain the propagating front and their rate of infection (viral adsorption) is concentration dependent. As the host fraction increases, the velocity begins to level out; the rate of viral replication is ever less able to compensate for the increased depletion of freely diffusing particles caused by adsorption to the hosts. As the host fraction is further increased, the volume occupied by the host, independent of its adsorption properties, serves increasingly as a barrier to viral diffusion and the propagation is correspondingly reduced.

It is debatable whether the reduced velocities observed at large host fractions should be solely attributed to the effects of hindered diffusion. They may be due to biochemical causes; for example, hosts at high densities may be less able, metabolically, to support viral replication. Indeed, the fact that most types of viruses do not grow continuously when plated on their hosts supports this notion. Thus, our model ignores host aging, not because we believe these effects are negligible, but because the detailed biochemical data required to adequately quantify these effects are to our knowledge not yet available. From a broader perspective, our model demonstrates clearly that the reduced velocities at large host fractions cannot be fully explained by the effects of free virus depletion under favorable adsorption conditions. The measured velocities in Fig. 3, *a* and *b* more sensitive to the host fraction than the velocities of Fig. 1, *a* and *b*. Our attempt to capture this effect by modifying the viral adsorption mechanism to allow for irreversible high-multiplicity adsorption has only effectively changed the scale of the yield factor Y, not the functional form of the host dependence. Thus, other effects such as hindered diffusion, reversible high-multiplicity adsorption or metabolic changes must play a significant role.

A better understanding of the biological and physicochemical factors governing viral propagation will help us not only to clarify the mechanisms which dominate under different conditions, but also to reliably predict the magnitude of the front velocity from independent experiments. Until then, many questions await answers.

How does the metabolic state of the cell affect its ability to adsorb and produce virus particles? How does the lysis-induced liberation of cytoplasmic fluids containing, for example, lysozyme, growth inhibitors, or proteases influence the infection of adjacent hosts? Hosts at the air/agar interface grow better than those at the agar/petri dish interface; how does the host gradient normal to the agar surface influence propagation in the radial direction?

A better understanding of the propagation process will also help us reduce the uncertainties which accompany our velocity determinations. We have made measurements after 12 h of growth over a 12 h period. After the first 12 h, the turbidity of the colony suspension appears constant, suggesting that the host has or is approaching a stationary growth state. However, measurements of velocities have revealed 30 percent increases over several days growth (J. Yin, unpublished observations). Plaque growth may be selecting for mutant viruses which propagate well; selected mutants should then, in principle, propagate with a constant velocity when grown under the conditions which lead to their selection. This remains to be tested.

By observing how perturbations targeted at points in the viral infection cycle lead to changes in plaque growth, we can hope to reinforce our theoretical bridge between the propagation velocity and the microscopic mechanisms. For example, different lines of polyoma virus have been found to form plaques varying two- to three-fold in size (26). The small-plaque variants adsorb more readily to their host than the large-plaque variants; moreover, a single amino acid substitution in the major capsid protein of the virus is correlated to the weak adsorption/small plaque phenotype (27). If Fig. 2 applied for polyoma virus and covered the range of experimentally accessible adsorption constants, we would predict, assuming plaque size correlated directly with velocity, that the small-plaque adsorption constant, K, would be greater than 10^{-2}; at lower values weaker adsorbing viruses would produce smaller, not larger plaques. Moreover, if we knew the host fracton was 0.2, we could use Fig. 2 and our knowledge of plaque size differences to deduce that the small- and large-plaque variants had adsorption constants of roughly 10^2 and 10^1, respectively.

This exercise of deducing adsorption constants from plaque measurements or vice versa illustrates the kinds of information needed for rigorous comparisons. First, because plaques do not necessarily begin growing simultaneously, velocities of the propagating fronts, when obtainable, are prefered over sizes of plaques. Second, it is important to know how the propagation depends on the host concentration. This requires collecting front velocities over a range of host fractions (corresponding in the examples presented here to a range of nutrient broth concentrations for the agar-immobilized hosts).

APPENDIX 1

Front velocity

Effect of plaque curvature on the velocity

Curvature effects on the propagation velocity are accounted for by retaining both terms which arise from viral diffusion. Rewriting Eq (2a):

$$\frac{\partial[V]}{\partial t} = D\frac{\partial^2[V]}{\partial r^2} + \frac{D}{r}\left(\frac{\partial[V]}{\partial r}\right) + f([V],[B],[I]), \quad \text{(A1)}$$

where $f([V],[B],[I])$ accounts for the reactions which produce and consume the diffusing virus particles. Assuming the decay length, $(D/k_2)^{1/2}\ 1/\xi$ is much less than r, (D/r) may be replaced in Eq. 2a by (D/R), where R is the plaque radius. As before, we look for a traveling-wave solution, with velocity $\bar{c}$, in the coordinate $\bar{z} = \bar{r} - \bar{c}\,\bar{t}$. This results in a modified form of the matrix in Eq. 3:

$$\begin{pmatrix} \xi^2 - \bar{c}(1+\gamma)\xi - \kappa_1 & 0 & \kappa_{-1} + Y \\ -\kappa_1 & \bar{c}\xi & \kappa_{-1} \\ \kappa_1 & 0 & -\bar{c}\xi - \kappa_{-1} - 1 \end{pmatrix} \begin{pmatrix} a_1 \\ a_2 \\ a_3 \end{pmatrix} = 0, \quad \text{(A2)}$$

where $\gamma = (D/k_2)^{1/2}/(R\bar{c})$ is the correlation for plaque curvature effects on the velocity. This system may be analyzed in the same way as Eq. 3 leading to polynomials with corrections of the form $(1 + \gamma)$, where γ becomes insignificant at large radii. Under typical experimental conditions ($D = 4 \times 10^{-8}$ cm^2/s and $c = 0.22$ mm/h) the effects of curvature are negligible for plaque radii greater than 0.1 mm.

Criteria for a positive solution to Eqs. 3 and 4

Because $Y > 1$ and κ_1 and κ_{-1} must be positive, $C_2 < 0$ and $C_3 > 0$, from Eq. 4. Furthermore, $C_3 = g(0) > 0$ and $g(-\infty) = -\infty$, so one of the roots of Eq. 4 is negative. For ξ real and positive, we require that at least one of the other two roots be real and positive. The nature of the three roots is determined by the discriminant of $g(\xi)$, $d \equiv (r_1 - r_2)^2 (r_2 - r_3)^2$, where r_1, r_2 and r_3 are the roots of $g(\xi)$. It may be verified that if $d \geq 0$, there are three real roots, and if $d < 0$, there is one real root and a complex conjugate pair. By Descartes' rule of signs (29) there are two positive roots for $d \geq 0$. Thus, $d \geq 0$ is a necessary and sufficient condition for the existence of a nontrivial solution to Eq. 3 with positive $\bar{c}$, ξ, a_1, a_2 and a_3; $d = 0$ is a minimal condition. As given elsewhere (28), this minimal condition can be reformulated in terms of the coefficients of Eq. 4: $d = -4C_1^3C_3 + C_1^2C_2^2 + 18C_1C_2C_3 - 4C_2^3 - 27C_3^2$.

For completeness, we also check that a_1, a_2, and a_3 have the same sign so that a solution with positive concentrations occurs. From Eq. 3, $\kappa_1 a_1 = (\bar{c}\xi + \kappa_{-1} + 1)a_3$, so a_1 and a_3 have the same sign. Substituting this expression into $-\kappa_1 a_1 + \bar{c}\xi a_2 + \kappa_{-1}a_3 = 0$ gives $\bar{c}\xi a_2 = (\bar{c}\xi + 1)a_3$, so a_2 and a_3 also have the same sign.

Conditions for the existence of traveling wave solutions

The existence of traveling wave profiles at velocities greater than $\bar{c}$, the minimum velocity, requires the connection of the desired leading front with a trailing front. The trailing front may be analyzed by letting $\bar{V} = \bar{V}_{-\infty} - a_1 \exp(\xi\bar{z})$, $\bar{B} = a_2 \exp(\xi\bar{z})$ and $\bar{I} = a_3 \exp(\xi\bar{z})$ to obtain analogous expressions to Eqs. 3 and 4 where the dimensionless

concentrations ($\overline{V}, \overline{B}, \overline{I}$) now approach ($\overline{V}_{-\infty}$, 0, 0) as $z \to -\infty$,

$$\begin{pmatrix} -\xi^2 - \bar{c}\xi & -\kappa_1 \overline{V}_{-\infty} & \kappa_{-1} + \mathrm{Y} \\ 0 & \bar{c}\xi - \kappa_1 \overline{V}_{-\infty} & \kappa_{-1} \\ 0 & \kappa_1 \overline{V}_{-\infty} & \bar{c}\xi - \kappa_{-1} - 1 \end{pmatrix} \begin{pmatrix} a_1 \\ a_2 \\ a_3 \end{pmatrix} = 0, \qquad \text{(A3)}$$

and

$$\xi(\xi + \bar{c})[\bar{c}^2\xi^2 - \bar{c}\xi(\kappa_{-1} + 1 + \kappa\overline{V}_{-\infty}) + \kappa_1 \overline{V}_{-\infty}] = 0. \qquad \text{(A4)}$$

The two positive real roots of Eq. A4 allow for trajectories converging to the stationary state at $\bar{z} = -\infty$, trajectories which are necessary for a complete traveling wave.

A complete solution of the traveling wave equations

$$\frac{\partial \overline{V}}{\partial \bar{z}} = \overline{W} \qquad \text{(A5}a\text{)}$$

$$\frac{\partial \overline{W}}{\partial \bar{z}} = -\bar{c}\overline{W} + \kappa_1 \overline{V}\overline{B} - (\kappa_{-1} + \mathrm{Y})\overline{I} \qquad \text{(A5}b\text{)}$$

$$\bar{c}\frac{\partial \overline{B}}{\partial \bar{z}} = \kappa_1 \overline{V}\overline{B} - \kappa_{-1}\overline{I} \qquad \text{(A5}c\text{)}$$

$$\bar{c}\frac{\partial \overline{I}}{\partial \bar{z}} = -\kappa_1 \overline{V}\overline{B} + (\kappa_{-1} + 1)\overline{I}, \qquad \text{(A5}d\text{)}$$

would prove the existence of trajectories connecting the homogeneous states (0, 0, 1, 0) at $\bar{z} = +\infty$ to ($\overline{V}_{-\infty}$, 0, 0, 0) at $\bar{z} = -\infty$ for the components vector ($\overline{V}, \overline{W}, \overline{B}, \overline{I}$). Here the introduction of $\overline{W} = \partial\overline{V}/\partial\bar{z}$ allows reduction of all equations to first order. In the absence of explicit integrals the existence proof is not straightforward. Proofs for somewhat simpler problems have been presented by Dunbar (30), and Kennedy and Aris (31). We conjecture that a general existence proof for multicomponent traveling waves, satisfying the velocity condition such as we have derived in the leading front, will be forthcoming in a wide class of similar models which will obviate the need for such specific proofs. Such a proof in the one-component case was provided by Kolmogorov (14). Nonetheless, we have been able to find one explicit integral of Eq. A5:

$$\overline{W} = -\bar{c}[\overline{V} - (\mathrm{Y} - 1)(1 - \overline{B}) + \mathrm{Y}\overline{I}], \qquad \text{(A6)}$$

leading to the three-component system,

$$\frac{\partial \overline{V}}{\partial \bar{z}} = -\bar{c}[\overline{V} - (\mathrm{Y} - 1)(1 - \overline{B}) + \mathrm{Y}\overline{I}] \qquad \text{(A7}a\text{)}$$

$$\bar{c}\frac{\partial \overline{B}}{\partial \bar{z}} = \kappa_1 \overline{V}\overline{B} - \kappa_{-1}\overline{I} \qquad \text{(A7}b\text{)}$$

$$\bar{c}\frac{\partial \overline{I}}{\partial \bar{z}} = \kappa_1 \overline{V}\overline{B} + (\kappa_{-1} + 1)\overline{I}. \qquad \text{(A7}c\text{)}$$

This is sufficient to determine $\overline{V}_{-\infty} = \mathrm{Y} - 1$ or $V_{-\infty} = (\mathrm{Y} - 1)B_0$; as expected, the concentration of viruses, $V_{-\infty}$, is readily obtained from the viral yield per host, Y, and the host concentration, B_0.

APPENDIX 2

Limiting cases

Slow adsorption

When the viral adsorption and desorption processes are slow relative to the death rate of the infected host (κ_{-1} small and fixed K) the b_3X and b_4 terms of Eq. 5 give a dominant balance:

$$c_{\mathrm{SA}} = 2[D(k_1 f B_{\max})(\mathrm{Y} - 1)]^{1/2}. \qquad \text{(A8)}$$

Fast adsorption

The case where adsorption is fast relative to the host death rate can be considered when Eq. 5 is reparametrized in terms of κ_1 and κ_{-1}, rather than K and κ_{-1}. For κ_1 large, the b_2X^2, b_3X and b_4 terms give a dominant balance:

$$c_{\mathrm{FA}} = \left(\frac{3D}{(k_1 f B_{\max})}\right)^{1/2}\left(\frac{3k_2\mathrm{Y}}{2}\right). \qquad \text{(A9)}$$

APPENDIX 3

Decay length

An expression for the decay length of the front, λ, may be obtained by noting that under the critical condition that a positive real root exists for Eq. 4, the first derivative with respect to $\xi = (D/k_2)^{1/2}(1/\lambda)$ must be zero. This can be combined with Eq. 4 to obtain an expression for the decay length as a function of the front velocity, the viral diffusivity and the kinetic parameters:

$$\lambda = \left(\frac{D}{k_2}\right)^{1/2}\left(\frac{2(C_1^2 - 3C_2)}{9C_3 - C_1C_2}\right), \qquad \text{(A10)}$$

where C_1, C_2 and C_3 are defined in Eq. 4. Under the limiting conditions previously considered, expressions for the decay length may also be calculated.

Equilibrated adsorption

$$\lambda_{\mathrm{EQ}} = \frac{2D}{c_{\mathrm{EQ}}(fK_{\max} + 1)}. \qquad \text{(A11)}$$

Slow adsorption

$$\lambda_{\mathrm{SA}} = \frac{2D}{c_{\mathrm{SA}}}. \qquad \text{(A12)}$$

Fast adsorption

$$\lambda_{\mathrm{FA}} = \frac{2c_{\mathrm{FA}}}{3k_2\mathrm{Y}}. \qquad \text{(A13)}$$

Large yield

$$\lambda_{\mathrm{Y}} = \frac{3D}{2c_{\mathrm{Y}}}. \qquad \text{(A14)}$$

APPENDIX 4

Glossary of Notation

a_1, a_2, a_3	positive constants (dimensionless);
$[B]$	concentration variable for host bacteria (1/ml);
B_0	constant concentration of host bacteria (1/ml);
B_{max}	maximum attainable value of B_0, value which completely fills the volume (1/ml);
c	velocity of propagation (mm/h);
c_{EQ}	velocity of propagation for the equilibrated-adsorption limit (mm/h);
c_{FA}	velocity of propagation for the fast-adsorption limit (mm/h);
c_{SA}	velocity of propagation for the slow-adsorption limit (mm/h);
c_Y	velocity of propagation for the large-yield limit (mm/h);
$\bar{c}$	$c/(k_2D)^{1/2}$, velocity of propagation (dimensionless);
C_1	$[(\kappa_{-1} + 1)/\bar{c} - \bar{c}]$ (dimensionless);
C_2	$-(\kappa_1 + \kappa_{-1} + 1)$ (dimensionless);
C_3	$\kappa_1(Y - 1)/\bar{c}$ (dimensionless);
D	diffusion coefficient for the virus (cm^2/s);
D_{eff}	$2(1 - f)D/(2 + f)$, diffusion coefficient for virus, accounting for the volume fraction occupied by the host (cm^2/s);
f	B_0/B_{max}, volume fraction occupied by host bacteria (dimensionless);
$[I]$	concentration variable for infected host bacteria (1/ml);
k_1	rate constant for virus adsorption to host (ml/s);
k_{-1}	rate constant for virus desorption from host (1/s);
k_2	rate constant for the death (lysis) of infected host (1/s);
K	κ_1/κ_{-1}, equilibrium adsorption constant (dimensionless);
K_{max}	k_1B_{max}/k_{-1}, maximum attainable value of K (dimensionless);
κ_1	k_1B_0/k_2, rate constant for virus adsorption to host (dimensionless);
κ_{-1}	k_{-1}/k_2, rate constant for virus desorption from host (dimensionless);
λ	$(D/k_2)^{1/2}/\xi$, decay length or width of front (mm);
r	radial-distance variable in polar coordinates (length);
$\bar{r}$	$(k_2/D)^{1/2}\,r$, radial-distance variable in polar coordinates (dimensionless);
R	plaque radius (mm);
t	time variable (time);
$\bar{t}$	(k_2t) time variable (dimensionless)
$[V]$	concentration variable for virus particles (1/ml)
X	$\bar{c}^2$ or $c^2/(k_2D)$ (dimensionless);
ξ	inverse of the decay length (dimensionless);
Y	yield factor of viruses per infected host bacterium (dimensionless);
z	$r - ct$, distance variable moving with velocity c (length);
$\bar{z}$	$(k_2/D)^{1/2}z$ or $\bar{r} - \bar{c}\bar{t}$, distance variable moving with velocity $\bar{c}$ (dimensionless).

We thank M. Eigen for his encouragement. M. Pop and C. Biebricher made helpful suggestions to the manuscript. F. W. Studier provided phage and host bacteria.

Dedicated to Manfred Eigen on the occasion of his 65th birthday.

Financial support from the Alexander von Humboldt Foundation, the Max-Planck-Society and the Bundes Ministerium für Forschung und Technologie (BMFT) is gratefully acknowledged.

Received for publication 26 September 1991 and in final form 30 December 1991.

REFERENCES

1. Domingo, E., D. Sabo, T. Taniguchi, and C. Weissmann. 1978. Nucleotide sequence heterogeneity of an RNA phage population. *Cell.* 13:735–744.
2. Studier, F. W. 1973. Genetic analysis of non-essential bacteriophage T7 genes. *J. Mol. Biol.* 79:227–236.
3. de la Torre, J. C., and J. J. Holland. 1990. RNA virus quasispecies populations can suppress vastly superior mutant progeny. *J. Virology.* 64:6278–6281.
4. Husimi, Y., K. Nishigaki, Y. Kinoshita, and T. Tanaka. 1982. Cellstat. A continuous culture system of a bacteriophage for the study of the mutation rate and selection process at the DNA level. *Rev. Sci. Instrum.* 53:517–522.
5. Kompier, R., J. Tramper, and J. M. Vlak. 1988. A continuous process for the production of baculovirus using insect-cell cultures. *Biotech. Lett.* 10:849–854.
6. von Angerer, K. 1924. Beiträge zum Bakteriophagenproblem. *Arch. f. Hyg.* 92:312–324.
7. Adams, M. H. 1959. Bacteriophages. Wiley Interscience, New York.
8. Cooper, P. D. 1961. The plaque assay of animal viruses. *Adv. Virus Res.* 8:319–378.
9. Symonds, N. 1958. The properties of a star mutant of phage T2. *J. Gen. Microbiol.* 18:330–345.
10. Parvin, J. D., A. Moscona, W. T. Pan, J. M. Leider, and P. Palese. 1986. Measurement of the mutation rates of animal viruses: influenza A virus and poliovirus type 1. *J. Virology.* 59:377–383.
11. Mayr-Harting, A. 1958. Die Entwicklung von Phagenlöchern und der Mechanismus der Phagenwirkung in festen Nährböden. *Zbt. f. Bakt. Paras. Infek. u. Hyg.* 171:380–392.
12. Koch, A. L. 1964. The growth of viral plaques during the enlargement phase. *J. Theoret. Biol.* 6:413–431.
13. Bauer, G. J., J. S. McCaskill, and H. Otten. 1989. Traveling waves of in vitro evolving RNA. *Proc. Natl. Acad. Sci. USA* 86:7937–7941.
14. Kolmogoroff, A., I. Petrovsky, and N. Piscounoff. 1937. Étude de l'équation de la diffusion avec croissance de la quantité de matière et son application à un problème biologique. *Moscow Univ. Bull. Math.* 1:1–25.
15. Bramson, M. 1988. Convergence to traveling waves for systems of Kolmogorov-like parabolic equations. *In* Non-linear Diffusion Equations and their Equilibrium States I. W.-M. Ni, L. Peletier, and J. Serrin, editors. Mathematical Sciences Research. Vol. 12. Springer Verlag, Berlin. 179–190.

16. Maxwell, J. C. 1873. A Treatise on Electricity and Magnetism. Vol. I. Clarendon Press, Oxford. 365.
17. Cussler, E. L. 1984. Diffusion, Mass Transfer in Fluid Systems. Cambridge University Press, Cambridge. 186–187.
18. Miller, J. H. 1972. Experiments in Molecular Genetics. Cold Spring Harbor Laboratory, Cold Spring Harbor, New York. 27–43.
19. Studier, F. W. 1969. The genetics and physiology of bacteriophage T7. *Virology.* 39:562–574.
20. Yin, J. 1991. A quantitative phenotype of viral propagation. *Biochem. Biophys. Res. Comm.* 174:1009–1014.
21. Delbrück, M. 1946. Bacterial viruses or bacteriophages. *Biol. Rev.* 21:30–40.
22. Krüger, D. H., W. Mann, S. Hansen, G. Bläsing, M. Bläsing, and C. Schroeder. 1988. A simple method of distinguishing the bacterial viruses T3 and T7, and a critical reevaluation of their heterologous and homologous exclusion. *J. Basic Microbiol.* 28:45–53.
23. Garen, A. 1954. Thermodynamic and kinetic studies on the attachment of T1 bacteriophage to bacteria. *Biochim. Biophys. Acta.* 14:163–172.
24. Ackermann, H.-W. 1976. La Classification des Phages Caudés des Entérobacteries. *Pathol. Biol.* 24:359.
25. Stollar, D., and L. Levine. 1963. Two-dimensional immunodiffusion. *Methods Enzymol.* VI:848–854.
26. Diamond, L., and L. V. Crawford. 1964. Some characteristics of large-plaque and small-plaque lines of polyoma virus. *Virology.* 22:235–244.
27. Freund, R., R. L. Garcea, R. Sahli, and T. L. Benjamin. 1991. A single amino-acid substitution in polyomavirus VP1 correlates with plaque size and hemagglutination behavior. *J. Virology.* 65:350–355.
28. Jacobson, N. 1974. Basic Algebra I. W. H. Freeman, San Francisco, 250–251.
29. Korn, G. A., and T. M. Korn. 1961. Mathematical Handbook for Scientists and Engineers. Second edition. McGraw-Hill Book Company, New York. 17.
30. Dunbar, S. R. 1983. Traveling wave solutions of diffusive Lotka-Volterra equations. *J. Math. Biology.* 17:11–32.
31. Kennedy, C. R. and R. Aris. 1980. Traveling waves in a simple population model involving growth and death. *Bull. Math. Biol.* 42:397–429.